







RESEARCH ARTICLE | SEPTEMBER 03 2025

## Dissecting the role of substrate folding in enzymatic digestion

Special Collection: [Biointerphases in India](#)

Nilimesh Das  ; Tanmoy Khan  ; Soumya Chaudhury  ; Bhaswati Sengupta  ; Pratik Sen  



*Biointerphases* 20, 051001 (2025)

<https://doi.org/10.1116/6.0004803>



View  
Online



Export  
Citation

### Articles You May Be Interested In

A folded substrate can slow down an enzymatic reaction

*Scilight* (September 2025)

Optimizing numerical performance of enzymatic coagulation models: Insight into proteolysis and gelation dynamics

*Physics of Fluids* (November 2024)

Nanodiamond-chymotrypsin and nanodiamond-papain conjugates, their synthesis and activity and visualization of their interaction with cells using optical and electron microscopy

*Biointerphases* (July 2017)



Advance your science and  
career as a member of

**AVS**

LEARN MORE



# Dissecting the role of substrate folding in enzymatic digestion



Cite as: *Biointerphases* 20, 051001 (2025); doi: [10.1116/6.0004803](https://doi.org/10.1116/6.0004803)

Submitted: 30 June 2025 · Accepted: 6 August 2025 ·

Published Online: 3 September 2025



Nilimesh Das,<sup>a),b)</sup> Tanmoy Khan,<sup>c)</sup> Soumya Chaudhury,<sup>d)</sup> Bhaswati Sengupta,<sup>e),f)</sup> and Pratik Sen<sup>g)</sup>

## AFFILIATIONS

Department of Chemistry, Indian Institute of Technology Kanpur, Kanpur, Uttar Pradesh 208 016, India

**Note:** This paper is part of the Biointerphases Special Topic Collection Biointerfaces in India.

<sup>a)</sup>[nilimesh.das@childrens.harvard.edu](mailto:nilimesh.das@childrens.harvard.edu)

<sup>b)</sup>**Present address:** Program in Cellular and Molecular Medicine, Boston Children's Hospital and Harvard Medical School, Boston, MA, USA.

<sup>c)</sup>[tanmoyk@iitk.ac.in](mailto:tanmoyk@iitk.ac.in)

<sup>d)</sup>[soumyac24@iitk.ac.in](mailto:soumyac24@iitk.ac.in)

<sup>e)</sup>[bhaswati1487@gmail.com](mailto:bhaswati1487@gmail.com)

<sup>f)</sup>**Present address:** Wexner Medical Center, Ohio State University, Columbus, OH 43210, USA.

<sup>g)</sup>**Author to whom correspondence should be addressed:** [psen@iitk.ac.in](mailto:psen@iitk.ac.in)

## ABSTRACT

The efficiency of enzymatic proteolysis is often attributed to the properties of the enzyme itself, with the substrate typically viewed as a passive participant. In this study, we demonstrate that the conformational state of the substrate critically influences proteolytic efficiency. Using human serum albumin (HSA) as a model substrate, papain as the enzyme, and urea as a controlled denaturing agent, we systematically investigated how substrate conformation might affect proteolysis. While papain maintains its structural and functional integrity across varying urea concentrations, HSA transitions through well-defined conformational states (native, compact intermediate, and unfolded), allowing us an opportunity to isolate the effects of the substrate structure. Utilizing site-specific fluorescent labeling and single-molecule fluorescence correlation spectroscopy, we monitor the progression of proteolysis. Our results show that digestion slows at 3M urea, where HSA adopts a compact form, and accelerates at 6M, where HSA takes on an unfolded state, compared to native HSA. These results reveal that substrate folding critically influences the digestion kinetics, probably by controlling protease accessibility and underscoring its importance in mechanistic enzymology and proteomics workflows.

Published under an exclusive license by the AVS. <https://doi.org/10.1116/6.0004803>

## I. INTRODUCTION

Protein digestion is a critical biological process, where enzymes target particular peptide bonds based on their sequence preferences.<sup>1–4</sup> For instance, trypsin exhibits selectivity for the carboxyl side of lysine and arginine,<sup>5</sup> chymotrypsin prefers aromatic residues such as phenylalanine and tyrosine, while pepsin exhibits broad specificity, favoring cleavage near hydrophobic residues at the N-terminus.<sup>6</sup> These cleavage preferences often define a characteristic proteolytic pattern for each enzyme. While the function of enzymes has long been studied in the context of their structure and dynamics,<sup>7–13</sup> the substrate protein is often treated as a static entity. Yet, proteins in their native folded state present a complex landscape

of the accessible and inaccessible peptide bonds, shaped by tertiary and quaternary structures.<sup>3,14</sup> Thus, even when an enzyme encounters multiple susceptible peptide bonds within a substrate, the enzymatic efficiency and the resulting proteolytic trajectory are influenced by the substrate's conformational state.<sup>15,16</sup> Despite extensive literature on enzymatic digestion for applications in proteomics and structural biology,<sup>1,3,17</sup> there is a noticeable scarcity of studies directly interrogating the effect of substrate conformational flexibility or denaturation on proteolytic outcomes. This gap is especially relevant considering the dynamic nature of the cellular environment, where proteins frequently undergo partial unfolding, ligand binding, or post-translational modifications that may influence their susceptibility to enzymatic attack.

09 October 2025 07:13:04

To address this, we focused on the enzymatic digestion of human serum albumin (HSA)—a large, multidomain plasma protein—using papain (a cysteine protease derived from papaya latex) (Fig. 1). Papain is a well-characterized enzyme and retains activity over a broad range of conditions, including moderate to high concentrations of urea and a wide range of temperatures.<sup>18,19</sup> This property provides a unique experimental advantage, i.e., it allows the structural state of the substrate to be modulated independently, without significantly perturbing the enzyme's activity or conformation.

In a previous study from our group, we established that the proteolysis of HSA by papain proceeds in a directional manner, and papain, among other enzymes, showed the highest efficiency of digestion.<sup>20</sup> We demonstrated that the cleavage pattern is not random but directed, likely due to differential accessibility or charge-based interactions at the domain surfaces. Building on that foundation, the present work aims to dissect how controlled conformational alterations of the substrate protein influence the efficiency and trajectory of enzymatic digestion.<sup>20</sup>

Here, we exploit the differential sensitivity of HSA and papain to urea. While HSA undergoes progressive unfolding at increasing urea concentrations,<sup>21</sup> papain remains structurally and functionally stable.<sup>18</sup> This unique combination allows us to examine how substrate conformation alone modulates proteolysis. Domain-III of HSA was selectively labeled with *p*-nitrophenyl coumarin ester (NPCE) at Tyr-411 residue.<sup>22–24</sup> The tagged HSA was subjected to digestion by papain under varying urea concentrations (0, 3, and 6M), and changes in fragment size were monitored using fluorescence correlation spectroscopy (FCS). Intriguingly, we observed an enhancement of proteolytic rate at denaturing urea concentration; however, at 3M, where the compact intermediate structure of HSA is evident, a slow digestion has been detected. These results underscore the critical yet underappreciated role of substrate conformation in governing enzymatic proteolysis. Our findings demonstrate that even in the absence of major changes to the enzyme, alterations in the structural landscape of the substrate can significantly modulate digestion kinetics.

## II. EXPERIMENT

### A. Materials and methods

HSA (fatty acid free), papain, tetramethylrhodamine-5-maleimide (TMR), cysteine hydrochloride, and disodium ethylenediaminetetraacetic acid (EDTA) were procured from Sigma-Aldrich (USA) and used without further purification. Analytical-grade disodium hydrogen

phosphate and sodium dihydrogen phosphate were obtained from Merck (India) and employed to prepare a 50 mM phosphate buffer (pH 7.4). Dialysis membrane with a 14 kDa molecular weight cut-off was purchased from Sigma-Aldrich and activated following the manufacturer's protocol prior to use. Centrifugal filtration unit (Amicon Ultra, 10 kDa MWCO) was sourced from Merck Millipore (Germany). High performance liquid chromatography (HPLC)-grade dimethyl sulfoxide (DMSO) was obtained from Finar Limited and used directly.

### B. Instrumentation and analysis

Steady-state absorption and fluorescence measurements were carried out using a double-beam UV-vis spectrophotometer (UV-2450, Shimadzu, Japan) and a spectrofluorimeter (FluoroMax-4, Jobin-Yvon, USA), respectively, with a 1 cm path length quartz cuvette.

Circular dichroism (CD) spectra measurements were carried out using a CD spectrometer (J-815, Jasco, Japan) employing a 0.2 cm quartz cuvette. The CDNN software was used to quantify the secondary structure content.<sup>25</sup>

FCS measurements were conducted using a laboratory-built confocal system, which has been described previously in many publications from our group.<sup>22,24,26,27</sup> The core instrumentation included an inverted confocal microscope (IX-71, Olympus, Japan) equipped with a 60× water-immersion objective (Numerical Aperture 1.2, UplanSApo, Olympus, Japan), a single-photon counting detector (SPCM-AQRH-13-FC, Excelitas Technologies, Canada), and a hardware correlator card (Flex99OEM-12/E, Correlator.com, USA). Samples were placed on standard glass cover slips (Blue Star, Polar Industrial Corp., India), positioned on the microscope stage. A 405 nm continuous-wave laser (MDL-III-405-5 mW, China) was focused approximately 40 μm above the surface of the coverslip to define the confocal detection volume. Emission photons collected by the objective were directed through a dichroic mirror (ZT405rdc, Chroma Technology Corp., USA) and an emission filter (FSQ-GG455, Newport, USA) and then coupled into a 25 μm core multimode optical fiber (M67L01, 0.10 NA, Thorlabs, USA) leading to the detector. Photon arrival times were autocorrelated using the correlator, and the data were visualized using a LABVIEW® interface. Proper control has been taken based on established protocols for the corrections of environmental effects such as viscosity and refractive index.<sup>22,27–29</sup>

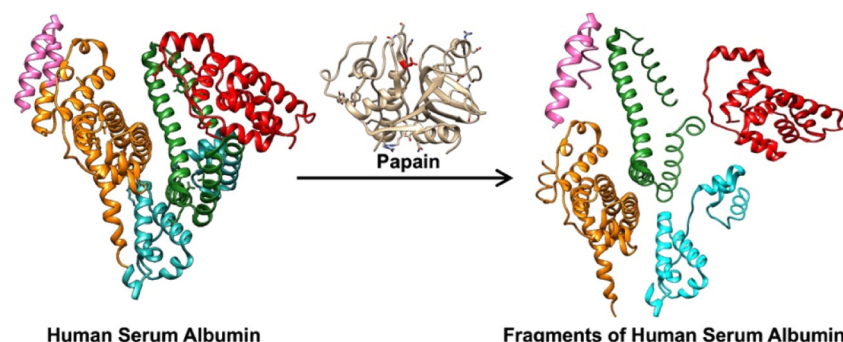


**FIG. 1.** Schematic representation of the digestion of HSA (PDB ID: 1HA2) by papain (PDB ID: 9PAP).

Under the assumption of Gaussian detection geometry and a single diffusing entity, the fluorescence fluctuation autocorrelation function is described by the following expression:<sup>28,30</sup>

$$G(\tau) = \frac{1}{N} \left(1 + \frac{\tau}{\tau_D}\right)^{-1} \left(1 + \frac{\omega^2 \tau}{\tau_D}\right)^{-1/2}. \quad (1)$$

In this equation,  $N$  represents the average number of fluorescent molecules in the detection volume,  $\tau_D$  denotes the characteristic diffusion time,  $\omega$  is the structure parameter or aspect ratio of the confocal volume, defined as  $\omega = r/l$ , which is the ratio of radial and axial radii of the Gaussian-shaped volume, respectively. To calibrate the detection volume geometry, we recorded autocorrelation curves for rhodamine 6G (R6G) in water across various concentrations. These curves were globally fitted using a known diffusion coefficient for R6G ( $D_t = 4.14 \times 10^{-6} \text{ cm}^2 \text{ s}^{-1}$ ) at 298 K.<sup>31</sup> Once the value of  $\omega$  was established through this calibration, it was held constant for all subsequent data fitting within the same experimental series.

In many cases, fluorescence intensity fluctuations arise not only from molecular diffusion but also from other dynamic processes. Under such conditions, the autocorrelation function expressed in Eq. (1) requires modification. A commonly used extension, accounting for an additional relaxation process, is given by<sup>28,30</sup>

$$G(\tau) = \frac{1}{N} \left(1 + \frac{\tau}{\tau_D}\right)^{-1} \left(1 + \frac{\omega^2 \tau}{\tau_D}\right)^{-1/2} \left(1 + a e^{-\frac{\tau}{\tau_R}}\right), \quad (2)$$

where  $\tau_R$  represents the characteristic relaxation time of the secondary process, while  $a$  denotes its relative amplitude. When multiple dynamic processes contribute to the fluorescence signal, further terms can be incorporated into the model accordingly. In our experiments, the optimal fitting function was chosen based on how well each model captured the observed data, and Eq. (2) turns out as a best possible model.

The translational diffusion coefficient ( $D_t$ ) of a molecule can be determined from its diffusion time ( $\tau_D$ ) and the radial dimension ( $r$ ) of the detection volume using the following relation:

$$D_t = \frac{r^2}{4\tau_D}. \quad (3)$$

Furthermore, the hydrodynamic radius ( $r_H$ ) is determined using the Stokes–Einstein equation as

$$r_H = \frac{k_B T}{6\pi\eta D_t}. \quad (4)$$

In the above equation,  $k_B$  denotes the Boltzmann constant,  $T$  represents the temperature in Kelvin, and  $\eta$  refers to the viscosity of the surrounding medium. In this work, the transverse dimension of the focal volume was estimated to be approximately 200 nm, corresponding to a detection volume of around 0.38 fl.

Following protein tagging, centrifugation was carried out at 5000 rpm using a refrigerated centrifuge. The tagged proteins were then lyophilized to obtain them in solid form using a standard freeze-drying setup.

### C. Labeling of HSA with CPM and NPCE

Site-directed fluorescent labeling of HSA was carried out using CPM and NPCE dyes, adapted from established methodologies with slight procedural adjustments [Figs. 2(a) and 2(b)].<sup>23,29,32,33</sup> CPM dye was conjugated to the sole accessible cysteine (cys-34) in domain-I of HSA,<sup>29</sup> whereas NPCE was selectively attached to the tyrosine-411 residue located in domain-III.<sup>23</sup> To begin, 40 mg of HSA was dissolved in 9.8 ml of phosphate buffer (50 mM), adjusted to pH  $\sim 7.4$  for CPM and  $\sim 8.0$  for NPCE. A 0.2 ml aliquot of dye stock solution (prepared in HPLC-grade DMSO) was added gradually with continuous stirring. Molar ratios were maintained at 1:1.2 for HSA:CPM to promote complete labeling and 1:0.9 for HSA:NPCE to minimize nonspecific or multiple site attachment.<sup>24</sup> After allowing the reaction to proceed for 10–12 h at 25 °C, the mixture was dialyzed at 5 °C against 1 l of phosphate buffer–DMSO mixture (15:1 v/v; 50 mM, pH 7.4), replacing the mixture four times daily over 4 days. This was followed by two medium exchanges within the next 24 h using only phosphate buffer to ensure removal of excess dye. The labeled protein was then concentrated using a centrifugal filtration unit with a 10 kDa molecular weight cut-off. Labeling efficiency, determined by the absorbance ratio of dye to protein, was approximately 88% for CPM and 70% for NPCE. Prior studies have shown that such dye conjugation does not significantly impact the structural or thermal stability of HSA, and thus, the labeled proteins were used without further modification in subsequent analyses.<sup>22,23,29</sup>

### D. Papain labeling with TMR and DACIA

To explore both active site accessibility and overall protein architecture, papain was selectively labeled with N-(7-dimethylamino-4-methylcoumarin-3-yl)iodoacetamide (DACIA) and Tetramethylrhodamine-5-maleimide (TMR) fluorescent dyes [Figs. 2(b) and 2(c)]. Papain is organized into two largely symmetrical regions, L and R, with the active site formed by a catalytic dyad (Cys-25 and His-159) nestled in the domain interface.<sup>34,35</sup> Active site labeling was performed by targeting Cys-25 with DACIA, following a modified version of the protocol described by Lindahl *et al.*<sup>36</sup> Briefly, papain was dissolved in Tris–HCl buffer (50 mM, pH 7.4) to a final concentration of 400  $\mu\text{M}$ , supplemented with 100 mM NaCl and 100  $\mu\text{M}$  EDTA. A DMSO solution of DACIA (0.58 mg in 1 ml DMSO) was slowly added to 9 ml of papain solution under gentle stirring while protecting from light. The mixture was incubated at 20–22 °C for 2 h and subsequently subjected to dialysis at 5 °C against 500 ml of phosphate buffer–DMSO mixture (1:15 v/v, 50 mM phosphate, pH 7.4) for 5 days. This was followed by an additional 5-day dialysis using only buffer. Postdialysis, the protein was concentrated via centrifugal filtration (10 kDa MWCO). For TMR conjugation, a standard labeling approach was followed.<sup>37,38</sup> Papain (90  $\mu\text{M}$ ) in phosphate buffer (50 mM, pH 7.4) was mixed with TMR dissolved in DMSO, maintaining a final dye-to-protein molar ratio of 3:1. The mixture underwent the same dialysis and lyophilization procedures as used for NPCE and 7-Diethylamino-3-(4-maleimidophenyl)-4-methylcoumarin (CPM)-labeled HSA. Based on previous validation studies, neither DACIA nor TMR attachment significantly affects the structural properties of papain.<sup>35,37,38</sup>

09 October 2025 07:13:04



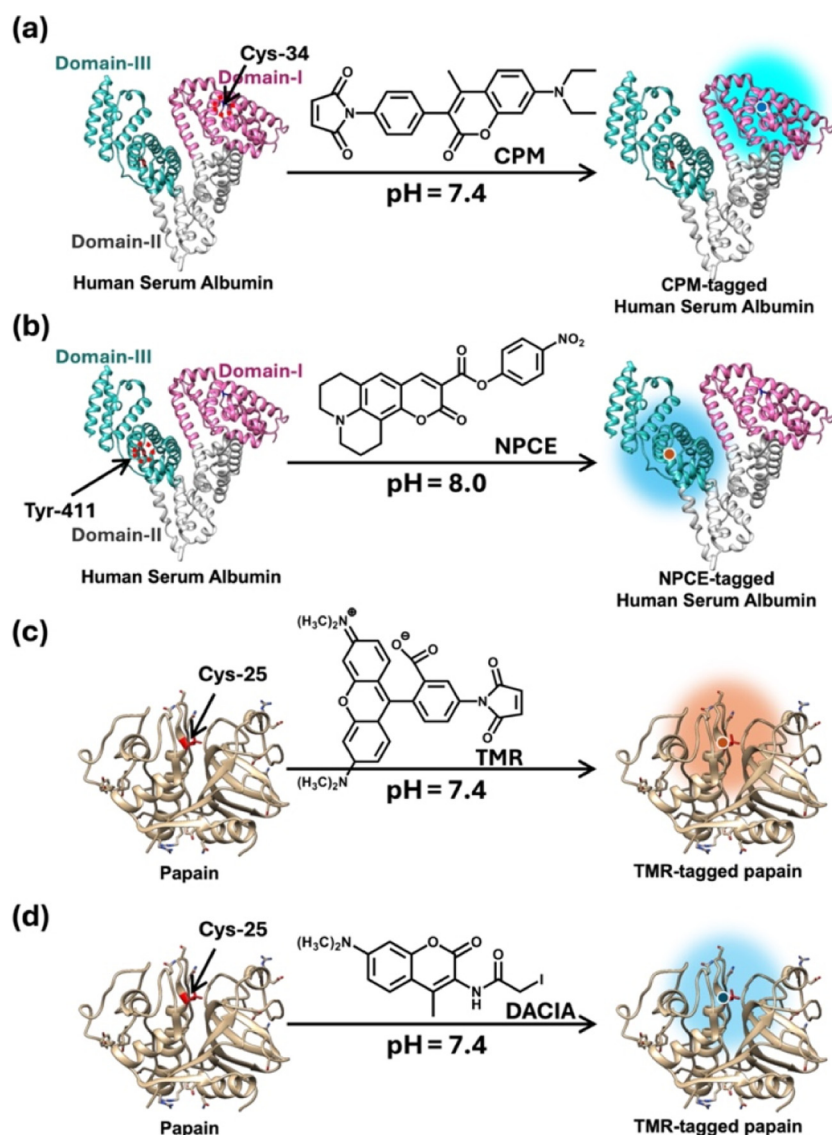


**FIG. 2.** Fluorescent tagging of proteins used in this study. (a) CPM labeling at Cys-34 residue of domain-I of HSA. (b) NPCE tagging at Tyr-411 of domain-III of HSA. (c) TMR tagging of Cys-26 residue of papain, and (d) DACIA labeling at the Cys-26 residue of papain. Cys-26 is present at the catalytic site of papain.

09 October 2025 07:13:04

### E. Sample preparation for digestion assay

To probe the digestion using FCS, we have exactly followed our previous publication.<sup>39</sup> First, unmodified papain was activated by incubation with cysteine and EDTA. Specifically, 0.1 ml of papain stock solution (10 mg/ml in phosphate buffer, pH 7) was added to 0.9 ml of activation buffer containing 1 mM EDTA and 10 mM cysteine hydrochloride, adjusted to pH 7. The mixture was then equilibrated at 37 °C for 10 min to promote full activation of the enzyme.<sup>39</sup> Digestion assays were carried out in a temperature-controlled water bath using a 1  $\mu$ M HSA solution. Activated papain was added from the stock to achieve the desired HSA-to-enzyme ratio. Prior to mixing, both enzyme and substrate solutions were equilibrated to the reaction temperature. At different definite time points, 20  $\mu$ l of aliquots was withdrawn

from the reaction mixture and immediately diluted to 200  $\mu$ l with ice-cold phosphate buffer to quench further enzymatic activity. The resulting diluted samples (corresponding to 100 nM HSA) were brought to room temperature and subsequently experimented employing FCS.

## III. RESULTS AND DISCUSSION

### A. Conformational modulation of papain in the presence of urea

Before investigating the role of substrate conformation in proteolysis, it is essential to assess the structural integrity of the enzyme itself under the denaturing conditions used. Steady-state fluorescence response of DACIA-tagged papain in the presence of

varying concentrations of urea has been analyzed for this purpose. No shift in the emission maxima of the DACIA-tagged papain was found up to ~7M urea [Fig. 3(a)], which suggests an almost similar tertiary structure of papain in the presence of urea, at least around the active site, where DACIA is tagged. The helicity for papain in the presence of urea was not calculated, as the measured CD spectra suffered from a low S/N ratio at wavelengths shorter than 210 nm. However, the measured CD spectrum of papain in the presence of 3 and 6M urea is almost similar to the spectrum obtained in buffer (see Fig. S1 in the [supplementary material](#)), which confirms a similar secondary structure of papain in the presence of up to 6M urea. The CD signal of papain at 208 and 222 nm against urea concentration is shown in Fig. 3(b). The result suggests that papain remains unperturbed up to 6M urea; however, beyond that, the secondary structure of papain starts breaking. We have also measured the hydrodynamic radii of the papain in the presence of urea employing FCS (see Fig. S1 in the [supplementary material](#) for the raw data). The hydrodynamic radii remain fairly constant up to 6M urea concentrations; however, beyond that, a slight increment in the hydrodynamic radius has been found [Fig. 3(c)]. This suggests a mild unfolding of papain in the presence of high concentrations of urea. However, Nakamura *et al.* have previously reported that the proteolytic activity of papain is retained up to 8M urea concentration, particularly when acting on protein substrates (casein).<sup>18</sup> Through spectroscopic studies, including CD and optical rotatory dispersion, they suggested no significant loss of  $\alpha$ -helicity or tertiary folding in papain in such high concentrations of urea.<sup>18</sup> This ensured that any variation in the observed proteolytic behavior in subsequent experiments could be attributed primarily to changes in the substrate conformation and not to enzyme inactivation.

Overall, our data show that papain retains its secondary and tertiary structures up to ~6M urea, with only mild unfolding at higher concentrations. These findings, along with prior reports of retained activity of papain up to 8M urea, confirm that variations in proteolysis observed under denaturing conditions would be due

to changes in substrate conformation and not due to enzyme conformation or activity.

## B. Conformational modulation of substrate (HSA) in the presence of urea

With the enzyme confirmed to remain structurally intact under denaturing conditions, we next examined how urea modulates the conformation of the substrate, i.e., HSA. HSA is well known to exhibit distinct conformational transitions in the presence of urea. HSA is a multidomain protein, and with the help of site-selective labeling and steady-state emission, we have investigated the urea-induced domain-wise conformational modulation of HSA [Fig. 4(a) and Fig. S2 in the [supplementary material](#)]. At lower concentrations of urea ( $\leq 2$ M), HSA retains much of its native conformation. Around 3M, it adopts a compact intermediate state and then progressively unfolds into extended and flexible conformations with increasing urea concentrations. The shift in the emission maxima originated from the domain-II distinctly points out that this compact state is populated at around 3–4M of urea. We have also followed the conformational transitions via CD and FCS study [Figs. 4(b) and 4(c) and Fig. S2 in the [supplementary material](#)]. The secondary structure of HSA ( $\alpha$ -helicity) remains almost similar up to 3M of urea and then progressively decreases with an increase in the urea concentration. The most compact state of HSA with the lowest hydrodynamic radius in the presence of urea has been observed at 3M urea employing FCS. Shil *et al.* also found such a compact state of HSA near such a concentration of urea, both in the presence and in the absence of sucrose.<sup>21</sup>

Overall, our data revealed that HSA retains its native structure up to ~2M urea, adopts a compact intermediate around 3M, and unfolds progressively at higher concentrations. These characterizations formed the basis for selecting three urea concentrations, 0, 3, and 6M, to represent native, compact intermediate, and unfolded states of HSA to explore the interplay between substrate folding and enzymatic processing.

09 October 2025 07:13:04

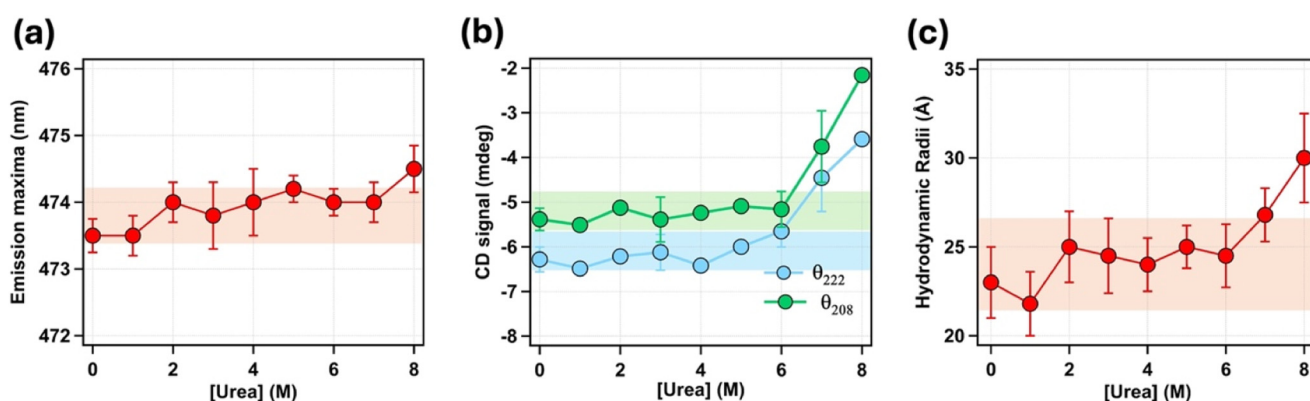


**FIG. 3.** Structural modulation of papain in the presence of urea. (a) Shift in fluorescence maxima of DACIA-labelled papain with increasing urea concentrations, showing almost no emission shift up to ~7M urea, (b) modulation of CD signal at 208 and 222 nm of papain against urea concentrations, showing no secondary structural change of papain up to 6M urea, and (c) hydrodynamic radius ( $R_h$ ) of papain measured by FCS. At least up to 6M urea, papain retains its secondary and tertiary structures. All the results are the average of three individual measurements, and the error bar represents the standard error of the mean.

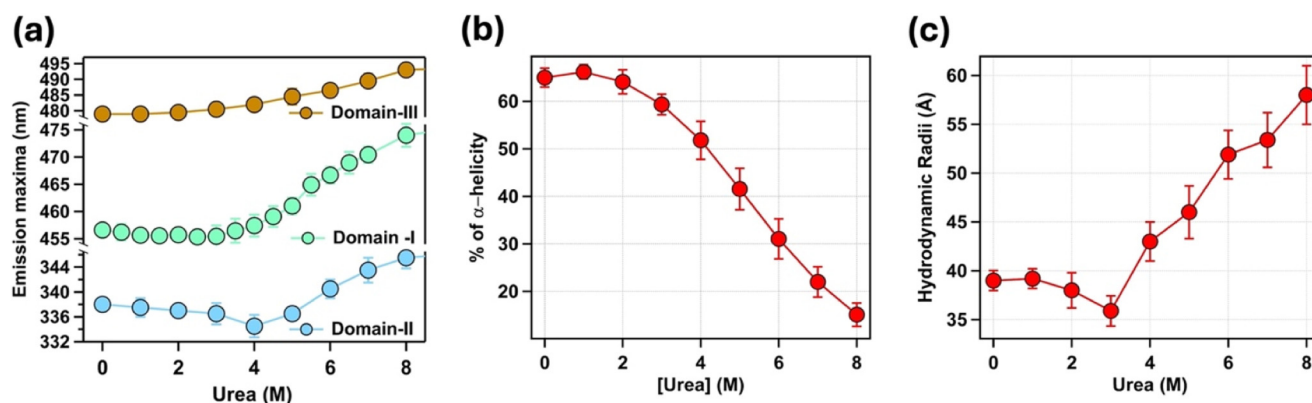


**FIG. 4.** Structural modulation of HSA in the presence of urea. (a) Shift in the fluorescence maxima of dyes labelled to different domains of HSA as a function of urea concentration: CPM (domain-I), intrinsic tryptophan emission (domain-II), and NPCE (domain-III). Emission from domains I and III remains same up to ~3M urea, followed by a red shift at higher concentrations. In contrast, domain-II shows a slight blue shift at ~3–4M urea before the red-shifting, indicating domain-specific structural responses. (b) Percent  $\alpha$ -helical content of HSA as a function of urea concentration from CD, indicating a gradual loss of secondary structure beyond ~2–3M urea. (c) Hydrodynamic radius ( $R_h$ ) of HSA measured by FCS, showing a compact intermediate at ~3M urea, before transitioning into a more elongated conformation at higher urea concentrations. All the results are the average of three individual measurements, and the error bar represents the standard error of the mean.

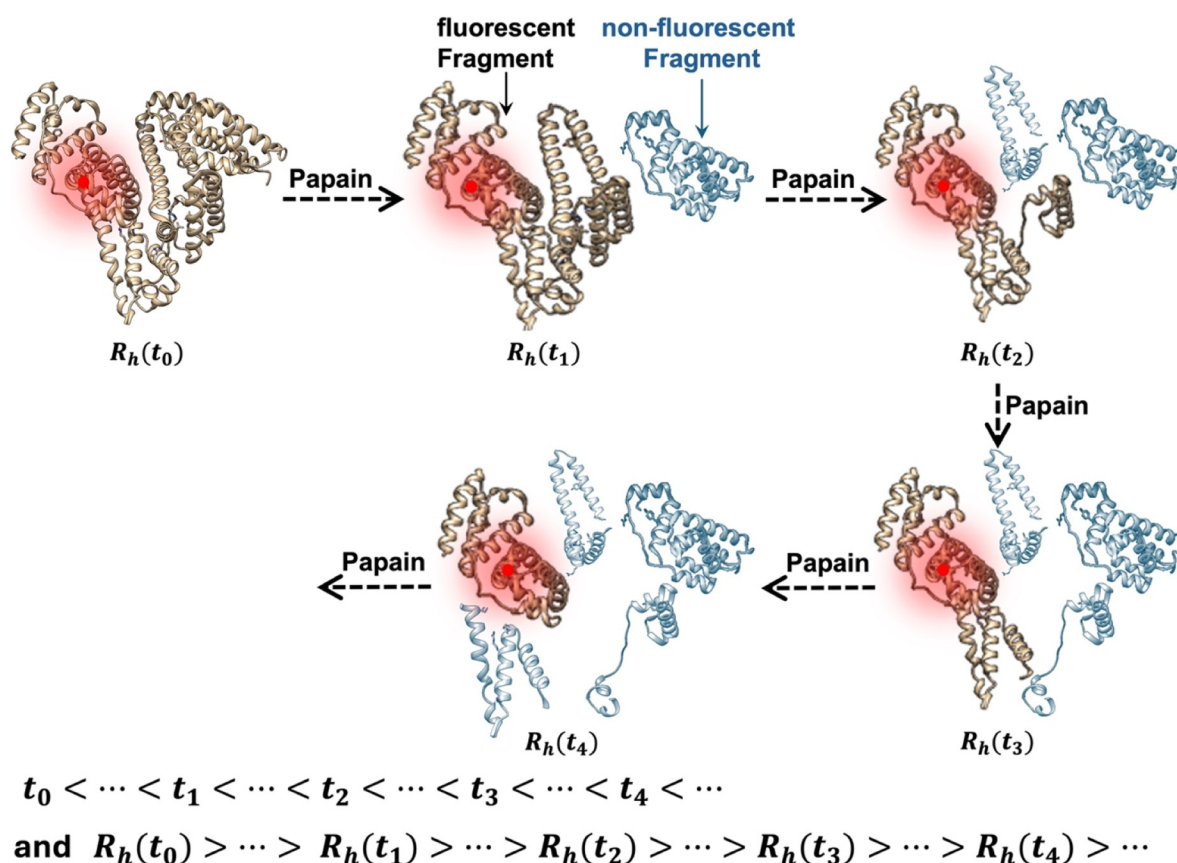


**FIG. 5.** Schematic representation for tracking of HSA digestion by papain employing FCS. The hydrodynamic radius of HSA fragments detected by FCS becomes progressively smaller with time because of digestion.

### C. Single-molecular-level tracking of proteolysis using FCS

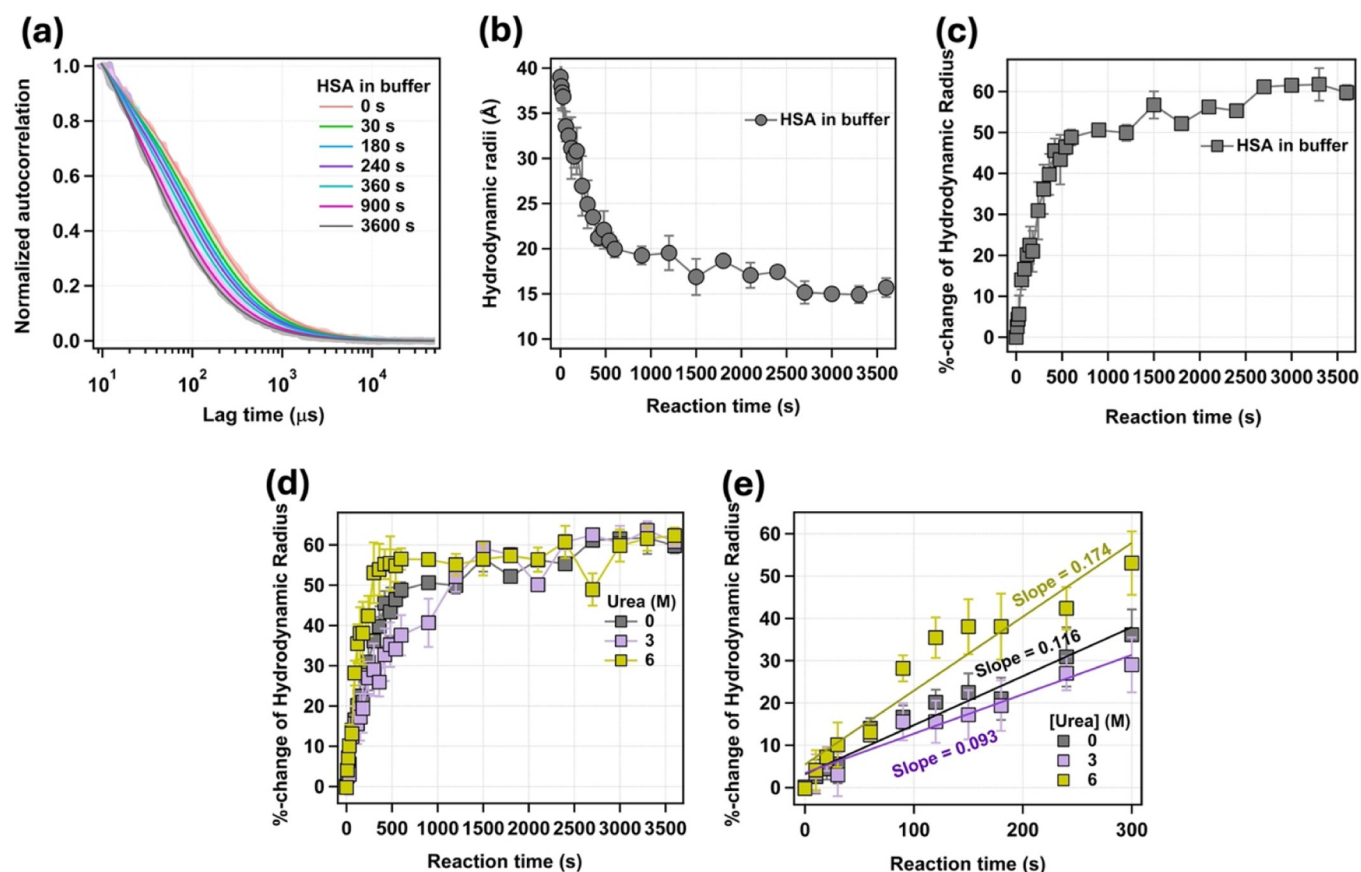
To probe the proteolysis, we have employed the single-molecular-level FCS technique, which we proposed a few years back.<sup>20</sup> HSA was site-specifically labeled at Tyr-411 (domain-III) using NPCE. Upon digestion by papain, cleavage of the protein near the labeling site results in a change in the diffusion behavior of the fluorescent fragment, which is easily detectable via FCS (Fig. 5). As shown in our earlier work, fluorescence tracking of HSA's domain-I via FCS revealed a more pronounced decline in hydrodynamic size than domain-III.<sup>20,40,41</sup> This finding strongly suggests a clear preference of the enzymes to begin digestion from the domain-I region of HSA.<sup>20</sup> Accordingly, in this study, we specifically tagged domain-III of HSA to monitor its enzymatic digestion.

FCS autocorrelation curves were acquired at regular time intervals during digestion, and the hydrodynamic radii of the fragment containing the fluorophore were determined from the diffusion time

fits. Figure 6(a) shows the FCS autocorrelation curves at different experimental time, which clearly suggests a time-dependent decrease of the diffusion time of the substrate fragment. A pure diffusion model could not adequately capture the behavior of any of the autocorrelation curves [Eq. (2)]. Fitting these curves with Eq. (3) yielded the hydrodynamic radius ( $R_h$ ) of the labeled fragment at different times [Fig. 6(b) and Fig. S3 in the supplementary material]. Next, to compare the digestion reaction at different urea concentrations, we have calculated the percent change in the hydrodynamic radius [Fig. 6(c)] as

$$\% \text{ change of hydrodynamic radii} = \frac{R_h(0) - R_h(t)}{R_h(0)} \times 100. \quad (5)$$

In the above equation,  $R_h(t)$  is the hydrodynamic radius of the fragments at any experimental time and  $R_h(0)$  is the hydrodynamics of the undigested HSA before the start of the reaction. From the initial slope of these curves [Fig. 6(e)], an idea about the rate of the



09 October 2025 07:13:04

**FIG. 6.** Digestion of HSA in the presence of urea. (a) Normalized autocorrelation curves of NPCE-labeled HSA fragments during papain digestion in buffer, recorded at various time points using FCS. (b) Hydrodynamic radius ( $R_h$ ) of the fluorescently tagged HSA fragments over time, showing progressive reduction due to proteolysis. (c) Percentage change in hydrodynamic radius over time, calculated using the equation X. (d) Comparison of percentage change in  $R_h$  over time in the presence of different urea concentrations (0, 3, and 6M), demonstrating urea-dependent modulation of digestion kinetics. (e) The early time digestion is presented to highlight the differences in initial digestion rates. Straight lines are the linear fits, and the slope is written for each trace in a color-coded manner.



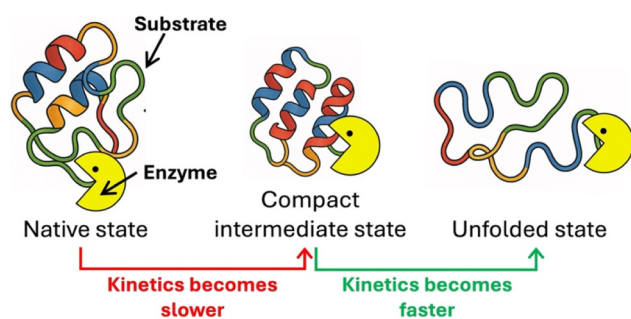


**FIG. 7.** Graphical summary depicting how substrate conformation influences proteolytic efficiency, emphasizing a slow digestion in the compact intermediate state and enhanced activity in the unfolded state.

reaction can be perceived. At 0M urea, digestion proceeds at a moderate rate with an initial slope of 0.116. In the presence of 3M urea, the rate was found to drop appreciably (the initial slope became 0.093). However, on increasing the urea concentration to 6M, a clear enhancement in the digestion rate is observed (the initial slope becomes 0.174).

Overall, using FCS, we found that papain-mediated digestion of HSA is slowest in the compact intermediate state (3M urea) and fastest in the unfolded state (6M urea), indicating that substrate conformation might affect the rate of proteolysis.

#### D. Role of substrate conformation in determining proteolytic efficiency

To understand how folding dynamics of the substrate influence enzymatic efficiency, we analyzed the relationship between HSA conformation and its susceptibility to proteolysis. Our findings clearly suggest that the conformational state of the substrate protein plays a pivotal role in modulating its digestion by an enzyme (Fig. 7). The slowdown of digestion at 3M urea correlates with previous reports of HSA adopting a molten globule-like compact intermediate at this concentration.<sup>21</sup> In such a state, while the protein is partially unfolded, hydrophobic residues may cluster to form a compact core, potentially shielding papain's cleavage sites. In contrast, at 6M urea, HSA is substantially denatured, with expanded conformations that enhance protease accessibility. The trend indicates that enzymatic efficiency does not scale monotonically with denaturation severity but instead depends on the structural presentation of cleavage sites, governed by dynamic substrate folding. This observation underscores the need to consider the substrate as an active determinant in enzyme-substrate interactions. Even when the enzyme structure and catalytic ability are held constant (as with papain in urea), substrate conformational changes alone can dramatically reshape digestion kinetics and trajectory.

#### IV. CONCLUSION

This study demonstrates that the conformational flexibility of a substrate protein is a crucial determinant of enzymatic digestion kinetics. By exploiting urea's contrasting impact on the conformations

of the enzyme (papain) and substrate (HSA), we show that papain-mediated proteolysis of HSA is not merely a function of enzyme activity but is intricately modulated by the substrate's folding state. The pronounced decrease in the digestion rate in the presence of 3M urea, which corresponds to a compact intermediate of HSA, contrasts with the enhanced rates at higher urea concentration (6M), where the protein is more unfolded. These results suggest a compelling case of substrate conformation-regulated enzymatic accessibility and efficiency and open new avenues for studying proteolysis in complex or partially folded protein systems. This might have broader implications in many fields, like for proteome workflows, where digestion efficiency may vary not just with enzyme conditions, but with subtle structural states of protein targets.

#### SUPPLEMENTARY MATERIAL

See the [supplementary material](#) for steady-state fluorescence, CD spectra, and normalized autocorrelation curves of HSA.

#### ACKNOWLEDGMENTS

N.D. and T.K. acknowledge the Council of Scientific and Industrial Research (CSIR), Government of India, and the Prime Minister Research Fellowship (PMRF), Government of India, respectively, for providing graduate fellowships. P.S. acknowledges the Indian Institute of Technology Kanpur for infrastructure and the Poonam and Prabhu Goel Chair position of IIT Kanpur for support. This work was financially supported by the Ministry of Education (MoE), Government of India (Grant No. MOE-STARS/STARS-2/2023-0215).

#### AUTHOR DECLARATIONS

##### Conflict of Interest

The authors have no conflicts to disclose.

##### Ethics Approval

Ethics approval is not required

##### Author Contributions

Nilimesh Das and Tanmoy Khan contributed equally to this paper.

**Nilimesh Das:** Conceptualization (equal); Data curation (equal); Formal analysis (equal); Writing – original draft (equal). **Tanmoy Khan:** Data curation (equal); Formal analysis (equal); Writing – original draft (equal); Writing – review & editing (equal). **Soumya Chaudhury:** Data curation (equal); Formal analysis (equal). **Bhaswati Sengupta:** Data curation (equal); Formal analysis (equal). **Pratik Sen:** Conceptualization (equal); Funding acquisition (equal); Supervision (equal); Validation (equal); Writing – review & editing (equal).

#### DATA AVAILABILITY

The data that support the findings of this study are available from the corresponding author upon reasonable request.

# REFERENCES

- <sup>1</sup>S. Vahdatpour, A. Pourrasmi-Mamaghani, M. S. Goloujeh, N. Maheri-Sis, H. Mahmoodpour, and T. Vahdatpour, *Electron. J. Biol.* **12**, 265 (2016).
- <sup>2</sup>H. J. Freeman and Y. S. Kim, *Annu. Rev. Med.* **29**, 99 (1978).
- <sup>3</sup>F. Kong and R. P. Singh, *J. Food Sci.* **73**, R67 (2008).
- <sup>4</sup>J. M. Berg, J. L. Tymoczko, and L. Stryer, *Biochemistry*, 5th ed. (W.H. Freeman Co, New York, 2002).
- <sup>5</sup>J. V. Olsen, S. E. Ong, and M. Mann, *Mol. Cell. Proteomics* **3**, 608 (2004).
- <sup>6</sup>G. J. C. Vreeke, J. P. Vincken, and P. A. Wierenga, *Food Res. Int.* **165**, 112485 (2023).
- <sup>7</sup>J. M. Yon, D. Perahia, and C. Ghélis, *Biochimie* **80**, 33 (1998).
- <sup>8</sup>N. Das, S. Yadav, K. S. Negi, E. Tarif, and P. Sen, *BBA Adv.* **2**, 100041 (2022).
- <sup>9</sup>T. Khan, N. Das, S. Bhowmik, K. S. Negi, and P. Sen, *J. Phys. Chem. B* **129**, 162 (2025).
- <sup>10</sup>T. Khan, B. Halder, N. Das, and P. Sen, *J. Phys. Chem. B* **128**, 8672 (2024).
- <sup>11</sup>K. R. Torgeson, M. W. Clarkson, D. Granata, K. Lindorff-Larsen, R. Page, and W. Peti, *Sci. Adv.* **8**, eabo5546 (2022).
- <sup>12</sup>S. L. Mader, A. Lopez, J. Lawatscheck, Q. Luo, D. A. Rutz, A. P. Gamiz-Hernandez, M. Sattler, J. Buchner, and V. R. I. Kaila, *Nat. Commun.* **11**, 1 (2020).
- <sup>13</sup>P. K. Agarwal, *Microb. Cell Fact.* **5**, 1 (2006).
- <sup>14</sup>D. L. Nelson, M. M. Cox, and A. A. Hoskins, *Lehninger Principles of Biochemistry* (Macmillan Learning, New York, 2021).
- <sup>15</sup>A. Rivera Del Rio, J. K. Keppler, R. M. Boom, and A. E. M. Janssen, *Food Funct.* **12**, 4570 (2021).
- <sup>16</sup>G. M. Cooper, *The Cell: A Molecular Approach*, 2nd ed. (Sinauer Associates, Sunderland, MA, 2000).
- <sup>17</sup>J. A. Mótyán, F. Tóth, and J. Tőzsér, *Biomolecules* **3**, 923 (2013).
- <sup>18</sup>K. Nakamura and M. Soejima, *Agric. Biol. Chem.* **34**, 489 (1970).
- <sup>19</sup>Z. Rashidi, A. Homaei, and R. Fernandez-Lafuente, *Process Biochem.* **146**, 147 (2024).
- <sup>20</sup>B. Sengupta, N. Das, V. Singh, A. K. Thakur, and P. Sen, *Int. J. Biol. Macromol.* **164**, 2524 (2020).
- <sup>21</sup>S. Shil, N. Das, B. Sengupta, and P. Sen, *ACS Omega* **3**, 16633 (2018).
- <sup>22</sup>N. Das and P. Sen, *J. Phys. Chem. B* **124**, 5858 (2020).
- <sup>23</sup>B. Sengupta, A. Acharyya, and P. Sen, *Phys. Chem. Chem. Phys.* **18**, 28548 (2016).
- <sup>24</sup>N. Das and P. Sen, *Phys. Chem. Chem. Phys.* **24**, 14242 (2022).
- <sup>25</sup>G. Böhm, R. Muhr, and R. Jaenicke, *Protein Eng., Des. Sel.* **5**, 191 (1992).
- <sup>26</sup>T. Khan, E. Tarif, Y. Awano, L. S. Lozada, N. Das, K. Tominaga, and P. Sen, *J. Mol. Liq.* **389**, 122882 (2023).
- <sup>27</sup>N. Das and P. Sen, *Biochemistry* **57**, 6078 (2018).
- <sup>28</sup>T. Wohland, S. Maiti, and R. Machán, *An Introduction to Fluorescence Correlation Spectroscopy* (IOP Publishing, Bristol, UK, 2020).
- <sup>29</sup>T. Khan, N. Das, K. S. Negi, S. Bhowmik, and P. Sen, *Int. J. Biol. Macromol.* **253**, 127100 (2023).
- <sup>30</sup>J. R. Lakowicz, *Principles of Fluorescence Spectroscopy* (Springer, New York, 2006).
- <sup>31</sup>C. B. Müller, A. Loman, V. Pacheco, F. Koberling, D. Willbold, W. Richtering, and J. Enderlein, *Europhys. Lett.* **83**, 46001 (2008).
- <sup>32</sup>N. Das, S. Sahu, T. Khan, and P. Sen, *Photochem. Photobiol.* **99**, 538 (2023).
- <sup>33</sup>R. Yadav, B. Sengupta, and P. Sen, *J. Phys. Chem. B* **118**, 5428 (2014).
- <sup>34</sup>J. Wang, Y. F. Xiang, and C. Lim, *Protein Eng., Des. Sel.* **7**, 75 (1994).
- <sup>35</sup>B. Sengupta, A. Chaudhuri, N. Das, and P. Sen, *Protein Pept. Lett.* **24**, 1073 (2017).
- <sup>36</sup>P. Lindahl, E. Raub-Segall, S. T. Olson, and I. Björk, *Biochem. J.* **276**, 387 (1991).
- <sup>37</sup>K. S. Negi, S. Rana, T. Khan, D. Mondal, and P. Sen, *Biophys. J.* **124**, 2082 (2025).
- <sup>38</sup>K. S. Negi, N. Das, T. Khan, and P. Sen, *Phys. Chem. Chem. Phys.* **25**, 32602 (2023).
- <sup>39</sup>E. Erez, D. Fass, and E. Bibi, *Nature* **459**, 371 (2009).
- <sup>40</sup>A. Berger and I. Schechter, *Philos. Trans. R. Soc. London. B* **257**, 249 (1970).
- <sup>41</sup>A. Lapolla, D. Fedele, R. Reitano, N. C. Aricò, R. Seraglia, P. Traldi, E. Marotta, and R. Tonani, *J. Am. Soc. Mass Spectrom.* **15**, 496 (2004).